THE AMERICAN SOCIETY OF MECHANICAL ENGINEERS
345 E. 47th St., New York, N.Y. 10017

94-GT-321

THEORETICAL AND EXPERIMENTAL INVESTIGATION OF CIRCUMFERENTIAL GROOVED CASING/HUB TREATMENT

Du Zhaohui
Department of Power Machinery Engineering
Shanghai Jiaotong University
Shanghai, China

Liu Zhiwei
Department of Aeroengines
Northwestern Polytechnical University
Xian, Shannxi, China

ABSTRACT

In this paper the 3-dimensional viscous numerical calculation is applied to explain the mechanism of extending stability of circumferential grooved casing and hub treatments. A new index which can quantitatively evaluate the ability to extend stability of circumferential grooved casing and hub treatments is proposed with flux of gas through the treatment grooves. The influences of the geometric parameters on improving stall margin are discussed. The conclusions are the same as those of experiments.

A circumferential grooved hub treatment is designed and tested beneath the stator blade row in a single stage axial flow compressor. The upstream and downstream 3-dimension flowfields are measured carefully in optimum operation condition and near stall margin condition by a combined three-hole probe and a mirco-five-hole probe which has 1.5mm diameter. It is shown that stall margin can be improved not only for the single stage compressor, but also for the rotor. Through a lot of experimental investigations and theoretical analyses, the mechanism of extending stability of circumferential grooved casing and hub treatments are systematic and comprehensive explained.

NOMENCLATURE

A_U, A_D, A_S, A_W	coefficients in the general finite
A_N, A_S, A_P	difference equations
G_1, G_2, G_3	convective terms normal to grid cell boundaries
M	Mach number
Re	Reynolds number
S^Φ	source term in the finite difference equation for the general scalar Φ
u, v, w	x, y, z components of the nondimensional velocities
x, y, z	nondimensional Cartesian coordinates
Γ^Φ	effective diffusity for the general scalar Φ
μ, μ_t	laminar and turbulent viscosities
ξ, η, ζ	nondimensional natural coordinates
η	efficiency
π	pressure ratio
ρ	density
Φ	general scalar quantity
$\bar{m}$	stall margin improvement
$\bar{n}$	relative rotating speed

INTRODUCTION

The study of casing treatment in the axial flow compressor has been carried out for more than 20 years, and has obtained remarkable achievements[1-7]. The results show that casing treatments have the ability to delay the appearance of compressor unsteady operation condition and to resist inlet distoring. But up to now the mechanism of improving stall margin remains poorly understood. Most of the investigations are carried out for an isolated rotor with casing treatment. It must be pointed out that in order to further explore mechanism of extending stability of casing treatment, hub treatment beneath stator blade row is a very helpful. This is because the effect of casing treatment over rotor row on stall margin improvement is similar to that of hub treatment beneath stator row on stall margin improvement, the difference being only that the direction of relative velocity is different. The hub treatment can simplify the structure, make the measure-

Presented at the International Gas Turbine and Aeroengine Congress and Exposition
The Hague, Netherlands — June 13–16, 1994

ment easy, and be suitable for exploring the mechanism of extending stability in greater depth.

The purpose of this paper is to further analyse the mechanism of extending stability of circumferential grooved casing and hub treatment by experimental measurements and numerical simulations.

The theoretical calculations and experimental researchs are very difficult because casing and hub treatments make the flowfields very complicated and the dimensions of treatment grooves are too small to be explored. Now there are many questions that can not be solved. This paper selects the circumferential grooved hub treatment as the research model. This is because the circumferential grooved hub treatment has relatively simple structure. On the basis of studing and analysing a lot of early works. It is thought that the viscosity and 3-D of flowfields are major cause affecting blade passage. So that 3-D, incompressible, steady, time average N-S equation, continuity and k-ε two equation turbulence model equation in general non-orthogonal curvilinear coordinates are applied to calculation the flowfields. In this paper the hub treatment with the circumferential treatment grooves is tested beneath the stator row in a single stage axial flow compressor. The upstream and downstream 3-D flowfields are measured carefully in optimum operation condition and near stall margin condition by a combined three-hole probe and a mirco-five-hole probe which has 1.5mm diameter.

NUMERICAL CALCULATION FORMULATION

Theoretical Formulation

Governing Equation. For steady mean flow, the time-averaged continuity equation and N-S equation in conjunction with the isotropic turbulent viscosity hypothesis are written in a Cartesian tensor form.

$$\frac{\partial \rho U_i}{\partial X_i}=0 \tag{1}$$

$$\frac{\partial \rho U_i U_j}{\partial X_i}=-\frac{\partial \rho}{\partial X_j}+\frac{\partial}{\partial X_i}[(\mu+\mu_t)(\frac{\partial U_i}{\partial X_j}+\frac{\partial U_j}{\partial X_i})-\rho\overline{U_iU_i}]+F_j \tag{2}$$

where ρ is the mean density, U_j is the mean velocity. From the k-ε turbulence model, the turbulent viscosity μ_t is given by

$$\mu_t=\rho C_\mu K^2/\varepsilon \tag{3}$$

where K is the turbulence Kinetic energy and ε is the turbulence energy dissipation.

The model is the composed of two equations, one for K and another for ε presented as follows:

$$\frac{\partial}{\partial X_i}(\rho U_i K)=\frac{\partial}{\partial X_i}(\frac{\mu_t}{\sigma_K}\frac{\partial K}{\partial X_i})+G-\rho\varepsilon \tag{4}$$

$$\frac{\partial}{\partial X_i}(\rho U_i \varepsilon)=\frac{\partial}{\partial X_i}(\frac{\mu_t}{\sigma_\varepsilon}\frac{\partial \varepsilon}{\partial X_i})+C_1\frac{\varepsilon}{K}G-\rho C_2\frac{\varepsilon^2}{K} \tag{5}$$

where G is the rate of production of turbulence kinetic energy.

This model contains five empirical constants which assume the following values:

$C_\mu=0.09$; $C_1=1.44$; $C_2=1.92$; $\sigma_K=1.0$; $\sigma_\varepsilon=1.3$

The wall function method is used in the present study to eliminate the large number of grid points needed to resovle the laminar sublayer. The following functions are used to bridge the near wall region.

$$K=\frac{\tau_w}{\rho C_\mu^{0.5}} \quad ; \quad \varepsilon=\frac{C_\mu^{3/4}K^{3/4}}{\kappa Z}$$

Here Z is the conventional coordinate normal to wall and τ_w is the wall shear stress. κ is the constant from the law of the wall with values of 0.41.

Transformation of Basic Equation.

The set of conservation equations typically can be written in the Cartesian system of coordinates for a scalar variable as:

$$\mathrm{div}(\rho\bar{U}\Phi-\Gamma^\Phi \mathrm{grad}\Phi)=S^\Phi \tag{6}$$

where Γ^Φ is an effective diffusion coefficient and S^Φ denotes the source term. When new independent variables ξ, η, ζ are introducted. Eq.6 changes according to the general transformation. $\xi=\xi(x,y,z)$, $\eta=\eta(x,y,z)$, $\zeta=\zeta(x,y,z)$. Partial derivatives of any function F are transformed according to

$$\begin{aligned}F^x&=\rho U\Phi-\Gamma^\Phi(j_{11}\Phi_\xi+j_{12}\Phi_\eta+j_{13}\Phi_\zeta)/J\\F^y&=\rho V\Phi-\Gamma^\Phi(j_{21}\Phi_\xi+j_{22}\Phi_\eta+j_{23}\Phi_\zeta)/J\\F^z&=\rho W\Phi-\Gamma^\Phi(j_{31}\Phi_\xi+j_{32}\Phi_\eta+j_{33}\Phi_\zeta/J\end{aligned} \tag{7}$$

$$\begin{aligned}F^\xi&=(j_{11}F^x+j_{21}F^y+j_{31}F^z)/J\\F^\eta&=(j_{12}F^x+j_{22}F^y+j_{32}F^z)/J\\F^\zeta&=(j_{13}F^x+j_{23}F^y+j_{33}F^z)/J\end{aligned} \tag{8}$$

where $j_{11}\sim j_{33}$ are transformation coefficients. J is Jacobian of transformation given by

$$J=\begin{vmatrix}X_\xi & X_\eta & X_\zeta\\ Y_\xi & Y_\eta & Y_\zeta\\ Z_\xi & Z_\eta & Z_\zeta\end{vmatrix} \tag{9}$$

So that Eq.6 can be written as fellow:

$$\frac{1}{J}(\frac{\partial(JF^\xi)}{\partial\xi}+\frac{\partial(JF^\eta)}{\partial\eta}+\frac{\partial(JF^\zeta)}{\partial\zeta})=S^\Phi \tag{10}$$

Method of Computation

General Transport Equation. In terms of the notation shown in Fig.1 (Taking the X-Y and ξ-η direction as a example) for a typical grid node P

enclosed in its cell and surrounded by its neighbors U,D,N,S, E and W, the finite difference approximation to the intergral conservation relation, Eq.9, over the cell is written as

$$\iint_A (JF^{\xi}\, d\zeta d\eta + JF^{\eta}\, d\zeta d\xi + JF^{\zeta}\, d\xi d\eta) = \iiint_v S^{\Phi} J d\xi d\zeta d\eta \quad (11)$$

In the present scheme, all flow properties are defined only at the nodes U,D,P,E,W,N,and S. After some linear interpolation and subsititution steps in physical plane, Eq.(11) can be changed to

$$A_P\Phi_P = A_U\Phi_U + A_D\Phi_D + A_E\Phi_E + A_W\Phi_W + A_N\Phi_N + A_S\Phi_S + S^{\Phi}_{NEW} \quad (12)$$

Where the coefficients A are shown as below. Taking U – D direction as a example

$$A_U = MAX(D_u + D_{\xi u} - D_{\xi w} + D_{\xi n} - D_{\xi s} - 0.5C_u, -C_u, 0)$$
$$A_D = MAX(D_d + D_{\xi w} - D_{\xi e} + D_{\xi n} - D_{\xi s} + 0.5C_d, \quad C_d, 0)$$
$$A_P = A_U + A_D + A_E + A_W + A_N + A_S$$
$$C_u = (\rho G_1 \Delta\eta\Delta\xi)_u; \qquad C_d = (\rho G_1 \Delta\eta\Delta\xi)_d$$
$$D_u = \left(\frac{\Gamma^{\Phi}}{J}\Delta\eta\Delta\xi/\delta\xi j_{11}'\right)_u; \qquad D_d = \left(\frac{\Gamma^{\Phi}}{J}\Delta\eta\Delta\xi/\delta\xi j_{11}'\right)_d$$
$$D_{\xi w} = 0.25\left(\frac{\Gamma^{\Phi}}{J}\Delta\xi j_{21}'\right)_w; \qquad D_{\xi e} = 0.25\left(\frac{\Gamma^{\Phi}}{J}\Delta\xi j_{21}'\right)_d$$
$$D_{\xi u} = 0.25\left(\frac{\Gamma^{\Phi}}{J}\Delta\eta j_{31}'\right)_u; \qquad D_{\xi d} = 0.25\left(\frac{\Gamma^{\Phi}}{J}\Delta\eta j_{31}'\right)_d$$
$$G_1 = j_{11}U + j_{21}V + j_{31}W \quad (13)$$

Pressure Correct Equation. For the original SIMPLE procedure, the prssure correction equation is shown as below. The details are shown in reference [8,9]

$$A_P P_P' = A_U P_U' + A_D P_D' + A_E P_E' + A_W P_W' + A_N P_N' + A_S P_S' + S_P \quad (14)$$

S_P represents the local imbalance of mass. Eq.(14) can be now solved with the some algorithm for Eq.(12) to yield the corrective pressure.

It has been learned from this pressure correction scheme with the ordinary grid arrangement, that the oscillatory pressure field is produced. This has been observed previously. The major source of this instability originated from the second – order centered $2\Delta x$ – difference approximation of the pressure gradient at the grid node. This scheme cannot sense the $1\Delta x$ – pressure oscillation. A staggered mesh was successfully used to remove these oscillations since the centered $1\Delta x$ – difference could be used for the pressure gradient with the staggered arrangement. However, this technique cannot be applied to the present method since the Cartesian velocity components u,v and w are not related to the grid line orientations. As an alternative approach, the scheme of Hirt et al.[10],where the pressure is defined in the center of cell, while u,v and w velocity components are defined at all corners, is introduced. In this case, pressure oscillation remained in the diagonal direction, and this scheme is equally unsuitable for the pressure purpose.

To eliminate the oscillations with pressure ordinary grid arrangement, a new treatment of the locally linearized convective terms, G1, G2, and G3 are introduced. It showld be remembered that these convective terms are always located on the cell boundaries and are obtained by interpolations between grid nodes. These interpolations are responsible for decoupling the velocity and pressure fields. If G_i^* are drived from Eq.(13). It would assume the expression

$$G_1^* = BP_\xi^* + \cdots\cdots \quad (15)$$

where all other terms are dropped for the convenience of discussion. Even though G1 is related to P in the form of Eq.15, the G1 value on the cell boundary is actually obtained from interpolation between the grid nodes. Thus the G1 value so determined cannot detect 1 $\delta\xi$ – pressure variation. One may remedy this situation by correcting the P_ξ' term through a $1\delta\xi$ difference scheme on the cell boundary. The effective form is found to be

$$G_{1u}^* = \overline{G_1^*} + \overline{B}\left(\frac{P_u^* - P_p^*}{\delta\xi} - \overline{P_\xi^*}\right) \quad (16)$$

where the overbar denotes the regular results obtained from linear interpolation between grid nodes U and P. The interpolated pressure gradient term P_ξ' based on the $2\delta\xi$ – center difference is replaced by the $1\delta\xi$ – center difference on the cell boundary. This procedure ensures strong velocity – pressure coupling. In some test cases, this procedure is proven to show better convergence behavior than the original SIMPLE procedure. It is worthwhile to note that this modification through Eq.(16) becomes redundant if the pressure varies linearly within the field.

The boundary condition required to solve the pressure correction equation is that the normal derivative of the pressure correctionis p' vanishes on the boundary in the computational plane. The actual pressure value on the boundary is established by extrapolation from interior values with the conditions of vanishing normal derivatives of pressure there.

RESULT AND DISCUSSION FOR NUMERICAL COMPUTATION

Computation Process

When the circumferential grooved hub treatment is applied to the compressor, the flowfields will become

very complicated. If every factor affecting the flowfield must be consided. It is so different that the problem can not be solved now. It is necessary to take some simplified steps.

In this paper it is assumption: 1>the flowfields are impressible; 2>the number of treatment grooves is two.

In computation three kinds of axial treatment position are consided. First the two treatment grooves are in the front part of the blade chord, second the two treatment grooves are in the middle part and third the two treatment grooves are in the back part. The Cartesian system coordinates and symbols are shown in Fig.2.

The parameters of axial position, depth and width of treatment grooves are shown in below.

1)axial position of treatment grooves(l/C)

position	front	middle	back
one	26%	46%	67%
two	42%	73%	93%

2)depth of grooves:

deeper: h/H=16%: shallower: h/H=7%

3)width of grooves:

wider: W/C=20% narrower: W/C=13%

In computation, the parameters of the stator blade geometry are the same as that described in the experiment part of this paper, but the clearance is zero. A $40\times15\times17$ grid is used and the $Re=4\times10^5$. The operation condition of compressor is near stall margin condition.

Physical Model of Circumferential Grooved Hub Treatment

Fig.3 is velocity vectors in Z-Y plane. This plane is at the 70% chord of stator balde. The h/H of treatment groove is 16%, and the w/c is 13%. It shows some phenomena. 1) Great changes have taken place in cascade passage when hub treatment is used. The ranges of change are in the limited of 20% span away from the stator hub. This phenomenon testifies the results of many early experiments. (the influence of circumferential grooved casing treatment on the flowfields is on the ranges of 30% span away from the rotor tip). 2) There exist a flow that enters the treatment grooves near the blade pressure side and comes out into cascade passage near the suction side. This is because the treatment grooves can connect suction side and pressure side, and can feel pressure difference between two sides. This moving flow which can blow over the lower energy gas which accumulate near the tip region of stator suction surface. So that it can delay the flowfield separation and onset of stall. The purpose of extending stability can be achieved.

Fig.4 is the change of velocity vectors in X-Y plane at different position of balde passage. The h/H of treatment groove is 16%, and w/c is 20%. In the position 2% away from the pressure side, there exist a flow which moves into treatment grooves apparently. In the position of 10% this trend decreases, but arriving the position 40% the trend disappears. It is to say that these exist no inducing velocities at the middle part of passage. In the position of 20% away from suction surface the moving flow enters the blade passage. It is shown in the Fig.4 the ranges of flow entering the treatment grooves is less than that coming out of treatment grooves.

Affecting of Treatment Groove on Stall Margin Improvement

In this paper a new index is proposed to evalute ability to improve stall margin in quantity. The new index is presented by the flux of gas through the treatment grooves $m=\int_A wdA$.(A is areas of connecting the pressure side with suction side. W is velocity moving from pressure side to suction side).

It must be pointed out that the flux in the table is gotten by theory calculation. In this paper authors do not measure the flux because the structure of treatment groove is too complicated to be measured.

Tab.1 the Change of flux

Groove	FWS	FWD	MWS	MWD	BWS	BWD
Flux	85	162	96	274	90	272
A	32	85	32	85	32	85
F/A	2.66	2.75	3.00	3.22	2.80	3.20
Groove	FNS	FND	MNS	MND	BNS	BND
Flux	30	126	64	206	26	111
A	38	86	38	86	38	86
F/A	0.79	1.47	1.68	2.29	0.68	1.29

F-Front; M-middle; B-back;
S-shallower; W-wider; N-narrower; D=deeper

It can be known from the table 1. 1)To the wider grooves series: The deeper grooves have stronger flux than shallower ones, but the effect is not clear. It is to say that the effect of the width of treatment grooves on the stall margin improvement are better than that of the depth of treatment grooves. 2)To the narrower grooves series: it is clear that the deeper grooves is stronger than shallower grooves, when they have same width. So that the depth is the most important cause for extending stability. It must pay attention to the depth of treatment grooves when the circumferential grooved casing or hub treatment is designed. 3)To the same

depth series: the wider grooves are stronger than narrower ones. 4)Position of treatment grooves at the front part or middle part of blade chord are better than those at back part of blade chord.

Comparsion with Experimental Results

In the Ref.[11] the depth of circumferential treatment grooves is varied from 0.318cm to 2.896cm. It need 9 treatment grooves to cover the all the blade chord. In the experiment the numbers and positions of treatment grooves are decided on table 2.

Tab.2 Droping of stall point mass flow (100%)

position	2-9	2-9	2-9	1-2	1-5	2-5	2-6	3-7	2-6
depth	0.318	1.143	2.896	1.143	1.143	1.143	1.143	1.143	0.318
70% $\bar{n}$	1.5	3.6	5.7	-0.6	2.8	4.2	5.8	5.5	3.9
100% $\bar{n}$	3.5	1.6	7.2	0	2.4	3.9	4.4	4.1	2.2

It can be seen from the table. To 2-9 treatment grooves. When the depth of treatment grooves is increased from 0.318 to 2.896, the dropping mass flow at stall margin point is from 3.5% to 7.2%. The similar results can be gotten when 2-6 treatment grooves are used(3.9% to 5.8%). It is to say that effect of the deeper treatment grooves on improving stall margin is better than shallower treatment ones for the same treatment positions. To same depth of treatment grooves 1.143cm, 2-6 and 3-7 treatment grooves are better that 1-2 and 1-5 ones. So that when circumferential treatment grooves are used to improve stall margin, the treatment positions should be in the middle part or the all part of the chord, and the mumbers of treatment grooves must be enough.

Fig.5 and Fig.6 are experimental results from the Ref. [4] which is completed on a single stage axial flow compressor of Tubormachinery Lab, Northwestern Polytechnical University. The compressor is the same as the one described in the experiment part of this paper. The dimensions of circumferential treatment grooves are A: depth=6mm, width depth=2mm; B: depth=9mm, width =2mm; C: depth=12mm, width=2mm; D: depth=6mm, width=3mm. It can be seen from the Fig.5 that if the depth of treatment grooves is increased, the stall margin is increased also. There the loss coefficient is defined as $(p_1^* - p_2^*)/0.5\rho U^2$ To same width, if the depth is increased, the loss coefficient will be increased. To the same depth, if width is increased, the loss coefficient will be increased.

The results of experiments are similar to ones of theory and computation analyses.

TEST EQUIPMENT AND METHOD OF EXPERIMENT

The experiments are carried out with a single stage axial flow compressor. Its design parameters are: blade tip speed 237m/s, mass flow rate 5.6kg/s, average total pressure ratio 1.26, adiabaic efficiency 0.92, relative tip Mach number 0.78, hub-tip ratio 0.61, aspect ratio 1.92, number of blade 30, tip solidity 0.96, stagger angle at average radius 47°. The tip clearance varies from 0.10cm to 0.15cm from blade to blade.

For simulating the CT over rotor tip, a circumferential HT is made beneath the stator hub(see Fig.7). The geometric parameters are selected and designed based on the theory analyses described above and early experimental works. The width of treatment groove is three times the depth of treatment groove. The chord/depth ratio is 3. The depth of treatment groove is 6mm. The width of treatment groove is 2mm. The number of treatment groove is 6. The tip clearance is 0. 1/mm.

At a fixed condition (relative rotating speed $\bar{n}=0.54$), the distributions of flowfield with soild wall (SW) and HT are measured carefully, specially its endwall secondary flowfield. The data are taken from 23 radial and 13 circumferiential stations. The methods of measurements are conventional.

There are two combined 3-hole-probe at the upstream, and downstream of rotor and a mirco-five-hole-probe which has 1.5mm diameter at the downstream of stator. The two kinds of probes are cablibrated from M=0.2 to M=0.7.

TEST RESULT AND DISCUSSION

Improvement of Performance

Overall Performance. In studying the effect of circumferential HT on the overall performance of axial flow compressor, three traditional items

$$\bar{m} = (G_m / G_{m} \times \pi_m^* / \pi_m^*) \times 100\%$$

$$\eta_m^* = (\eta_m^* / \eta_{m}^* - 1) \times 100\%$$

$$\eta_m^* = (\eta_m^* / \eta_{m}^* - 1) \times 100\%$$

are used and their values are listed in the following table.

so: near stall margin condition of solid wall
ss: near stall margin condition of casing treatment
mo: optimum efficiency condition of solid wall
ms: optimum efficiency condition of casing treatment
rm: most change
rs: change near the stall margin condition.

It can be seen from the table that at $\bar{n}=0.54$, $\bar{m}$ is increased by 2.96%, the efficiency is decreased by 1.3%. Because the compressor used in this experiment stalls

first on the rotor tip, the effect of improving stall margin is not remarkable. If the inlet angle of stator is increased to make the stall appear first at the stator hub, the effect will be remarkable. The experimental results of this paper are shown in Ref[4]. A similiar conclusion was given by Cheng[1].

Tab.3 Change of single stage performance

Type	Gcor	π^*	$\bar{m}$	η^*_m	η^*_n
SW	2.863	1.0651	0	0	0
HT	2.783	1.0660	2.96%	−3.1%	−1.3%

Fig.8 is the comparsion of overall performance of HT with that of SW. It shows the mass flow moves to left and becomes small when HT is used. So it can delay the onset of stall. But at steady operation condition, the curves for HT and SW are similar. Through treatment the curves of pressure ratio − mass flow move left.

Element Performance. For the same inlet condition, the curves relating total pressure to pitch, at 2%, 10%, 45%,75% span away from the stator hub respectively, are shown in Fig.9. The data are taken from the exit of stator blade. Total pressures at all 4 span positions always have two distinct regions: main flow region and loss flow region. At the 2% span position the total pressure for HT is much higher than that for SW. Similar phenomenon exists at the 10% span position. At the 75% span position. The effect of HT is little because this position is far away from the HT. Through hub treatment the loss region shiftes from suction surface to pressure surface.

Tab.4 Change of rotor performance

Type	Gcor	π^*	$\bar{m}$	η^*_m	η^*_n
SW	2.863	1.0568	0	0	0
HT	2.783	1.0577	2.79%	−2.2%	−1.6%

Rotor Performance. It can be seen from the Tab.4 above that $\bar{m}$ is increased by 2.79% and efficiency is decreased by 2.2%. The data indicate that the change of the rotor performance is the same as that of single stage comprssor. The rotor performance are measured by the probes between the stator and rotor when the HT is used beneath the stator blade row at the same time.

Analysis of Experimental Results of Stator Blade Downflow

Experimental measurements are made in order to compare the downstream flowfields of HT with that of SW. The authors employ a mirco − five − hole probe to make detailed measurement of flowfields. Two conditions are selected: optimum efficiency operation condition and near stall margin condition, $\bar{n} = 0.54$.

Contour lines of total pressure are shown in Fig.10(a, b,c). The optimum efficiency condition of solid wall is (a), (b) is near stall margin condition of SW,(c) is near stall margin condition of HT. In optimum condition (a) the flowfields distribute well. The total pressure is lower in the regions of the endwall and blade tail. There is a hump in tail by the effect of variable work and isentropic.(The blades used in the test are designed by variable work and isentropic). The total pressure increases from tip to end of stator, and is relative lower at the up − endwall region. This phenomenon reflects the effect of the rotor tip stall on the stator blade passage. It can be explained by the knowledge that the blades have ability to absorb the tail[12]. There exists a lowest total pressure region near the stator tip. It shows this region has the strongest loss.

When closing to stall margin condition the position of tail keeps the same. It can be seen obviously there is a lowest pressure core which number is 1.038 at the position1/3 span away from the hub and close to the suction side of the blade. The endwall is dangerous region and it could be origin of stall or separation. It indicated this time it is going to stall, and the endwall stall is probable major cause[7].

But when the circumferential groove HT is applied, this lower pressure core transfers to middle part of blade passage and leaves the suction surface to mainflow. The number of total pressure increases to 1.042. On the effecting of circumferential and radial inducting velocities[12] the tail hump leave blade. The lower pressure core remains at the stator endwall yet. In mainflow the change of total pressure is the same as above. The appearance of the phenomenon is because the circumferential treatment grooves have induced the circumferential and radial velocities and made the lower energy flow move away from the stator hub region. It can delay the onset of stall.

CONCLUSION

The main conclusions of this paper are:

<1>The compressor with HT beneath the stator can not only imitate the CT over the rotor tip, but also improve stall margin of a single stage axial flow compressor.

<2>The 3D viscous numerical simulation is used to explain the mechanism of extending stability of circumferential grooved casing and hub treatments. In this paper a new index which can quantitatively evaluate the ability to improve stall margin for axial flow compressor is proposed with the flux of gas through the

circumferential treatment grooves. With the index the influences of structure parameters of treatment grooves on improving stall margin are discussed. The conclusions are the same as that of experiments.

<3>Through a lot of theoretical analyses and experimental investigations, the mechanism of extending stability of circumferential grooved casing and hub treatments are systematic and comprehensive explained. There exist a pressure difference between the pressure side and suction side of blade. A strong flow which can be absorbed in pressure side and poured out in suction side that can blow over the lower energy boundary layer that accumulates at the corner of blade. So that it can delay the stall appearance.

REFERENCE

1. Cheng,P., and Greitzer,E.M."Effect of Compressor Hub Treatment on Stator Stall and Pressure Rise", Journal of Aircraft, Vol.21, No.7, 1984, pp469 – 475.
2. Simth,G.D.J. and Cumpsty,N.A., "The Phenomena in Compressor Casing Treatment", ASME Journal of Gas Turbine and Power, Vol.107, No.3. 1984, pp532 – 541.
3. Treaster,A.L. and Yocum,A.M., "The Calibration and Application of Five – Hole – Probes", ISA Transactions, Vol.18, No.3, 1987, pp23 – 34.
4. Du Zhaohui, "Theoretical and Experiment Investigation of Grooved Casing Treatment in Axial Flow Compressor", Ph.D Thesis, Northwestern Polytechnical University, 1992.
5. Smith,G.D.J., "Casing Treatment in an Axial Compressor", Ph.D. Thesis,University of Cambridge, 1980.
6. Johnson,M.C., and Greitzer,E.M., "Effect of Slotted Hub and Casing Treatment on Compressor Endwall Flowfield",ASME Paper 86 – GT – 247, 1986.
7. Greitzer,E.M.,"A Fundamental Cirterion for Application of Rotor Casing Treatment", ASME Journal of Fluid Engineering, Vol.101, No.7, 1979, pp237 – 243.
8. Partankar,S.V.,"Numerical Heat Transfer and Fluid Flow", Hemisphere Publishing Corporation, Washington, 1980.
9. Rhie,C.M., and Chow,W.L., "Numerical Study of Turbulent Flow Past an Airfoil with Trailing Edge Separating, AIAA Jour., Vol.21,No.11, 1983, pp1525 – 1532.
10. Hirt,C.W., et al "An Arbitray Lagrangian – Eulerian Computing Method for All Flow Speed", Journal of Computational Physics, Vol.14; No.3, 1974, pp227 – 253.
11. Bailey,E.E.,"Effects of Grooved Casing Treatment on the Flow Range Capability of a Single Stage Axial Flow Compressor",NASA TMX – 2459, 1972.
12. Prince,D.C., Wisler,D.C,Hilvers,D.E., "Study of casing treatment Stall Margin Improvenment Phenomena", NASA CR – 134552, 1974.

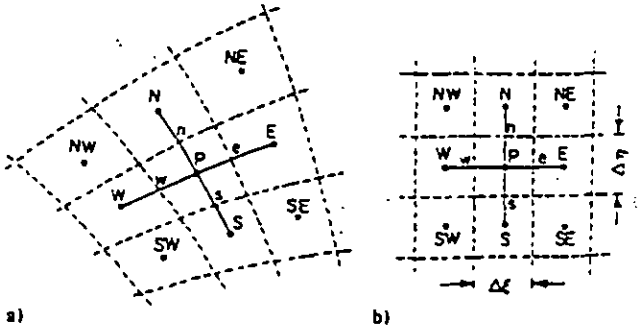

Fig.1 Finite difference grid representation.
a)Physical plane b)Transformed plane

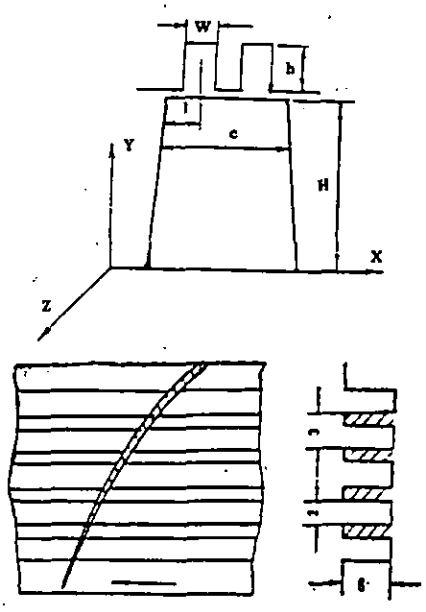

Fig.2 Structure of circumferential grooved hub treatment

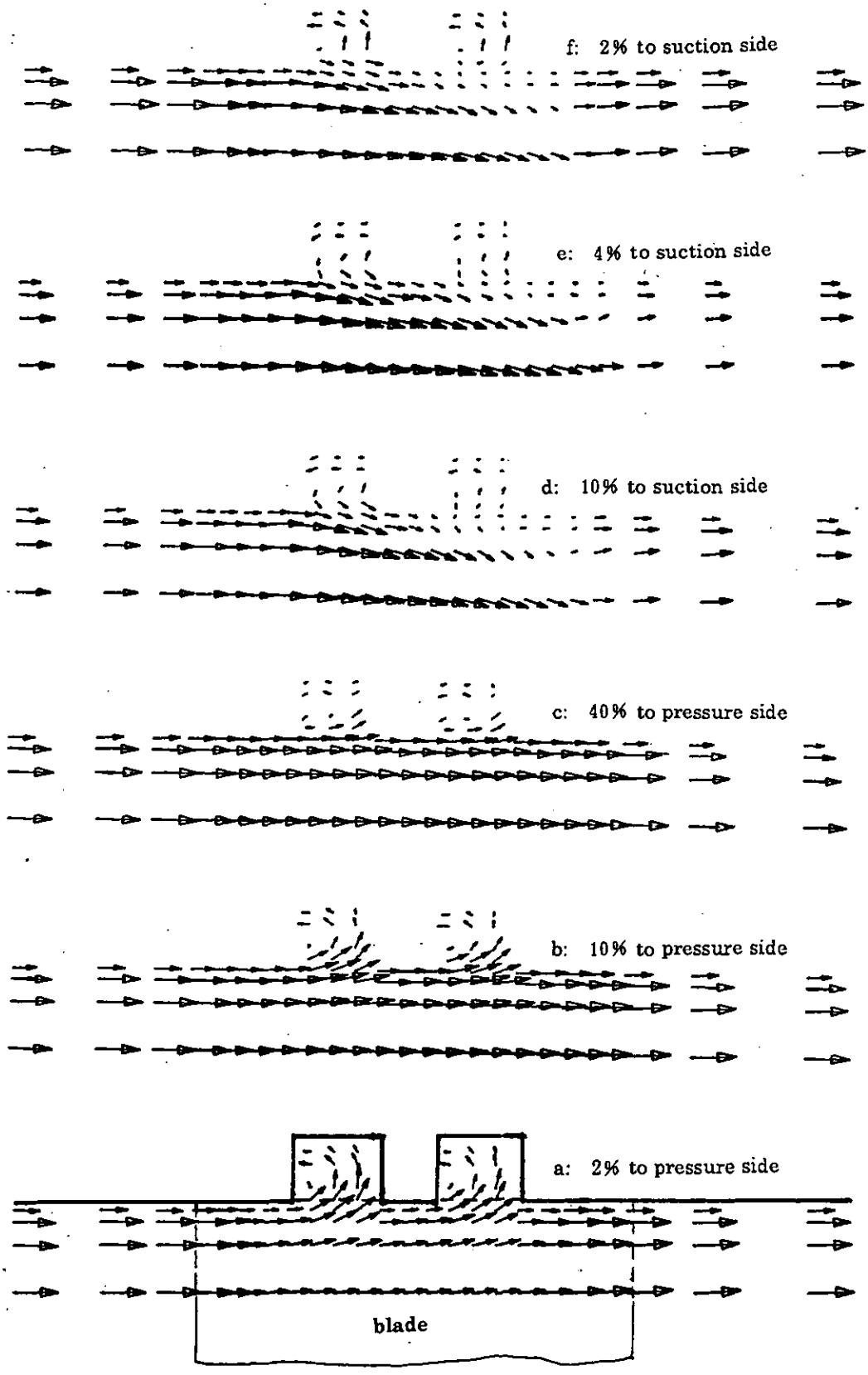

Fig.4 Velocity vector in X−Y plane

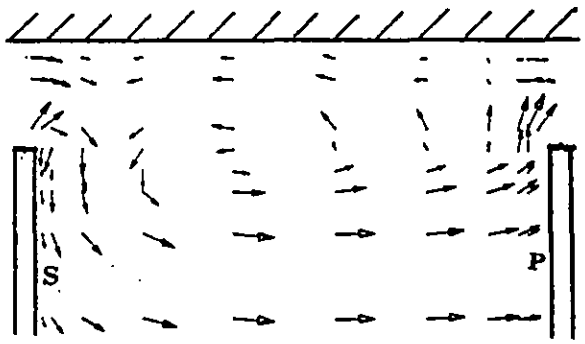

Fig.3 Velocity vector in Z—Y plane

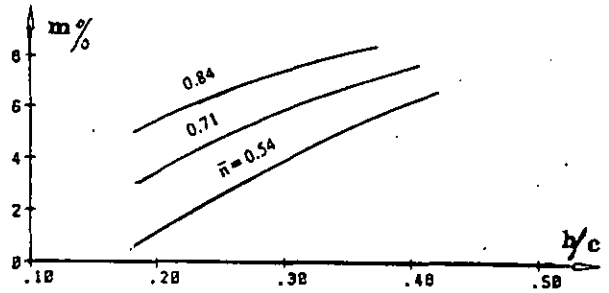

Fig.5 Stall margin improvement with groove depth

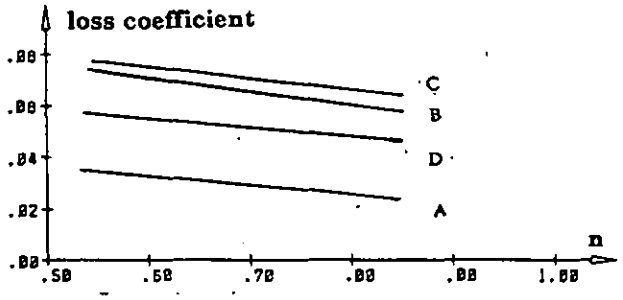

Fig.6 Variation of loss coefficient with groove depth

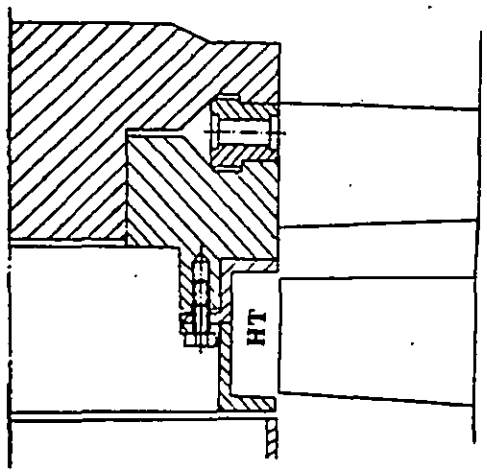

Fig.7 Cross section of axial flow compressor

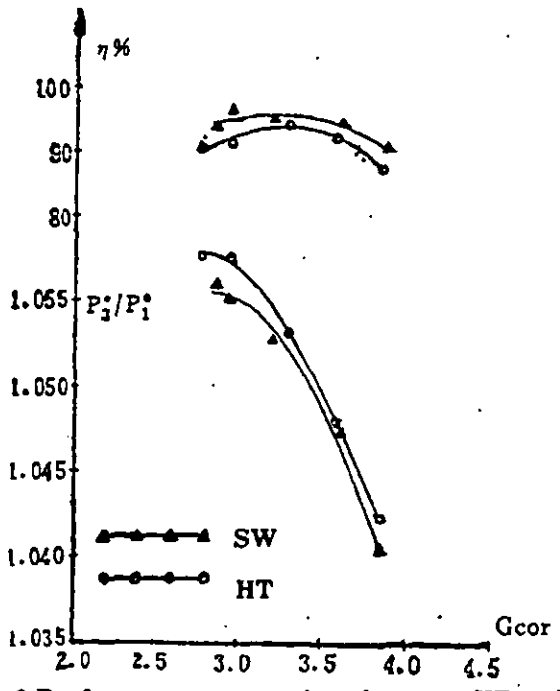

Fig.8 Performance comparison between HT and SW

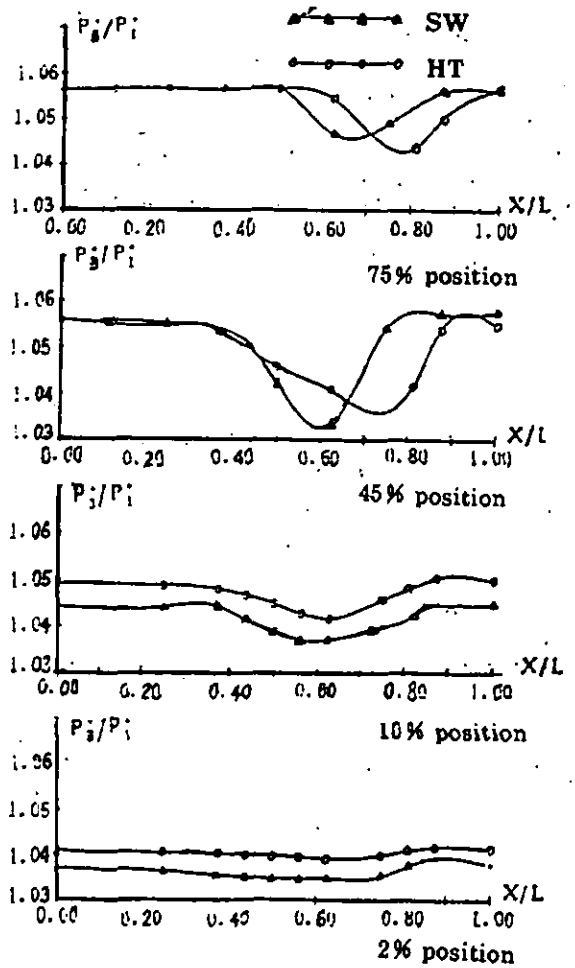

Fig.9 Variation of total pressure with pitch

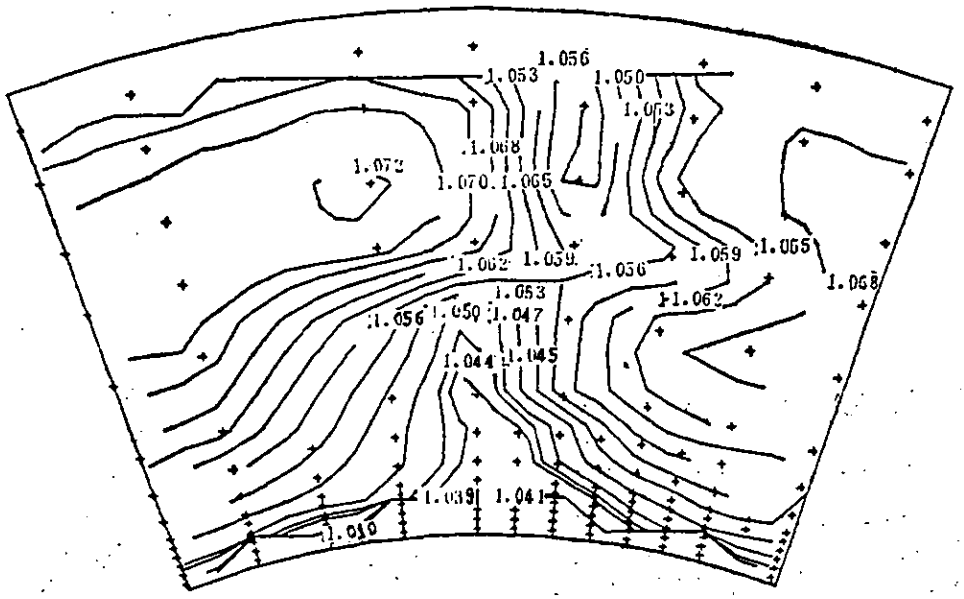

Fig.10(a) Contour of total pressure (design condition of SW)

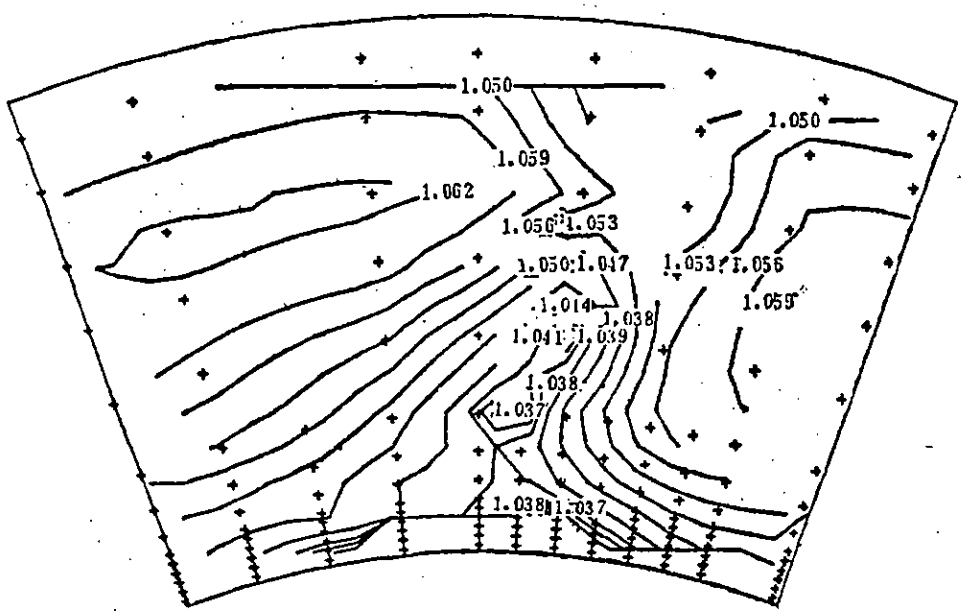

Fig.10(b) Contour of total pressure (stall margin condition of SW)

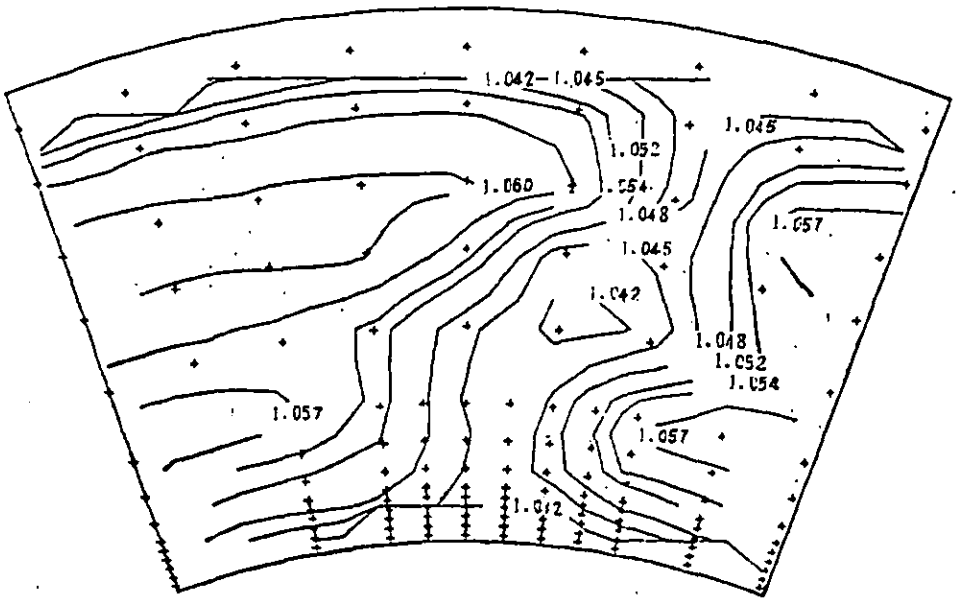

Fig.10(c) Contour of total pressure (stall margin condition of HT)